Optik - International Journal for Light and Electron Optics 242 (2021) 167305

Contents lists available at ScienceDirect

Optik - International Journal for Light and Electron Optics

journal homepage: www.elsevier.com/locate/ijleo

Original Research Article

Performances characterization of unsaturated polyester resin/polymethylmethacrylate waveguide for refractive index measurement

Ian Yulianti *, N.M. Darma Putra, Fianti, A.L. Dewi, D. Paradita

Physics Department, Faculty of Mathematics and Natural Sciences, Universitas Negeri Semarang, Sekaran, Gunungpati, Semarang, Central Java, Indonesia

ARTICLE INFO

Keywords:
Optical sensor
Optical waveguide
Refractive index

ABSTRACT

Investigation of refractive index (RI) and temperature response of unsaturated polyester resin (UPR)/polymethylmethacrylate (PMMA) based waveguides is presented. Three type waveguide structures were fabricated which are straight waveguide (sensor A), curved waveguide (sensor B) and half-filled core waveguide (sensor C). Simple fabrications were done by engraving PMMA sheets using CNC engraving machine to form grooves with cross section of 1×1 mm^2. The grooves were then filled with UPR as core material. To investigate the RI response, the waveguides were immersed in glucose solution with various concentration values having RI of 1.33 to 1.3547. Meanwhile, for temperature response characterization, the sensors were placed in distilled water while heated using magnetic stirrer with temperature variation of 35°C-85°C with increment of 5°C. The results showed that the sensors showed good RI sensitivity and linearity with the highest sensitivity of -48.476 dB/RIU. It was also observed that the sensors were temperature dependent. The highest error due to temperature effect is -1.8×10^{-4} RIU/°C.

1. Introduction

Measurement of refractive index (RI) is the main key in chemical, biological and physical parameters determination such as glucose concentration [1], milk fat content [2], humidity [3] and biomedical application [4]. Among various methods for RI measurement, optical RI sensor is interesting since it can be used in hazardous environment and is independent from electromagnetic interference. Optical sensors could be realized using optical fiber by applying various techniques such as phase modulation, intensity modulation and wavelength modulation technique. Phase modulation-based optical sensors for RI measurement have been developed using interferometer technique such as RI sensor fiber interferometer [5], fiber in-line Michelson interferometer [6] and Mach–Zehnder interferometer (MZI) [7]. Meanwhile, wavelength modulation-based sensors have been reported using surface plasmon resonance (SPR) technique [8,9] and grating [10–12]. Most of optical fiber sensors use silica single mode fiber (SMF). SMF is commonly used in telecommunication since it has low loss. However, for sensor application, very often SMF needs to be modified using various treatment such as etching, coating, and splicing that alter its structure and dimension. The change of structure and dimension due to such treatments makes the SMF fragile.

Another interesting optical sensor is optical waveguide-based sensor. Optical waveguide sensor (OWS) has advantages of robustness and could be integrated with other devices in single substrate. Like optical fiber sensors, OWSs have also been proposed for various applications such as magnetic field sensor [13], biosensor [14] and temperature [15]. For RI measurement, various OWSs

* Corresponding author.
E-mail address: ianyulianti@mail.unnes.ac.id (I. Yulianti).

https://doi.org/10.1016/j.ijleo.2021.167305
Received 18 April 2021; Accepted 22 May 2021
Available online 28 May 2021

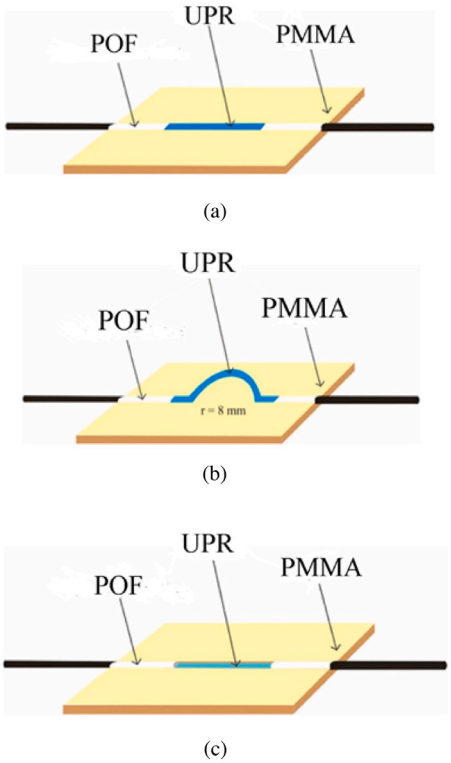

Fig. 1. UPR/PMMA SC-waveguide designs: straight waveguide (a), curved waveguide (b) and half filled-core waveguide (c).

have been developed. Ma et al. [16] simulated horizontal slot waveguide which was designed as Mach–Zehnder Interferometer (MZI) and Microring Resonator (MRR) for RI measurement. The sensors provide high sensitivity which were 17 024 nm/RIU and 177 nm/RIU for MZI based sensor and MRR based sensor, respectively. Wang et al. [17] used Graphene Oxide-Polymethyl Methacrylate (GO-PMMA) waveguide using intensity modulation technique. Both sensors used infrared light source in the range of 1520 nm–1570 nm. However, infrared could causes high absorption when it is applied for liquid RI measurement [18]. Ji et al. [19,20] investigate theoretically surface plasmon resonance (SPR) based RI sensor using gold cladded-epoxy waveguide in wavelength range of 800 nm–1000 nm. The wavelength range operation was chosen to minimize optical absorption.

Optical absorption could be further minimized by using visible light due to its low absorption coefficient in this wavelength range [21]. We have designed and fabricated optical waveguide for operation in visible light using polymethylmethacrylate (PMMA) with unsaturated polyester resin (UPR) as the core material [22]. PMMA and UPR were used since they have good transparency, durable and low cost. The waveguide was designed to be square core (BSC) waveguide to minimize coupling loss when it is connected to plastic optical fiber (POF). Other advantages of the UPR/PMMA-BSC waveguide is the low cost and simplicity in fabrication. Simulation on BSC waveguide response to RI has been done [23]. It was found that waveguide without upper cladding (square core waveguide, SC waveguide) provided highest sensitivity. The result is reasonable since removing the upper cladding allow the evanescent wave to interact with the environment. However, experimental study in investigating the SC waveguide response to RI has not been carried out. Moreover, since polymer has relatively high thermo-optic coefficient (TOC), environment temperature might contribute to the waveguide output intensity. Hence, it is important to characterize the sensor performance in terms of temperature response. Therefore, in this work, we fabricated UPR/PMMA based-SC waveguide and characterized their performances in terms of RI response and temperature response. Performance investigations were carried out for three waveguide structures which are straight waveguide, curved waveguide, and half-filled core waveguide.

2. Fabrication and characterization method

RI measurement of the UPR/PMMA based-SC waveguide sensor is based on the evanescent wave attenuation dependent to RI of the environment. By letting the upper surface of the waveguide uncladded, the evanescent wave is exposed to the environment. Therefore, the evanescent wave attenuation highly depends on the RI of the environment. Since the evanescent wave attenuation results in waveguide output intensity attenuation, then the RI could be measured by observing the change of the output intensity.

Beside using straight waveguide, other waveguide shapes and structures could be adopted to obtain higher sensitivity. Curved waveguide and half-filled core waveguide have good potential in improving sensor sensitivity [24–26]. At curved segment, more

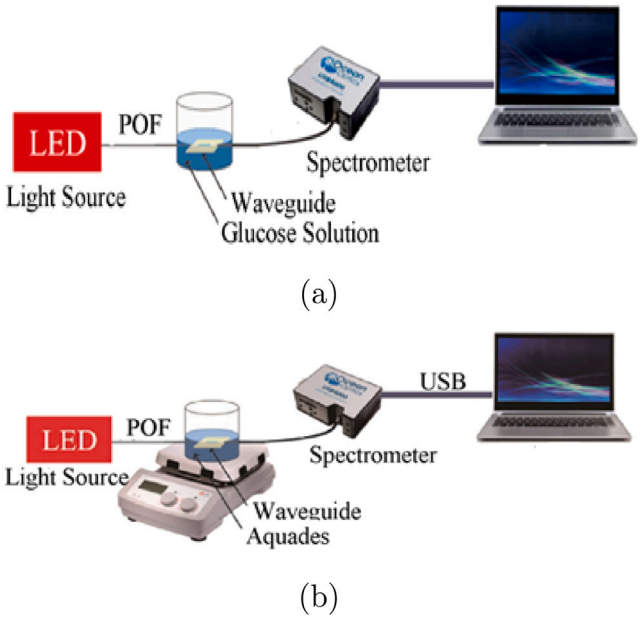

Fig. 2. Characterization set up for RI response (a) and temperature response (b).

light radiates to the environment since the light modes strike the interface of the core/cladding with an angle that less than critical angle. Hence, more light modes interact with the environment. In this work, we fabricated three waveguide structures which were straight waveguide (sensor A), curved waveguide (sensor B) and half-filled waveguide (sensor C), as shown in Fig. 1.

Waveguide fabrications were done by engraving PMMA sheet using CNC machine forming a groove with cross section of 1 × 1 mm^2 before filled with UPR as core material as described in [22]. The RI of PMMA and UPR are 1.4905 and 1.566, respectively. The waveguide length of sensor A and C are 3 cm and the curvature of waveguide B is 8 mm. After the waveguide core was filled with UPR, the waveguide was stored in room temperature until the UPR solidified. The upper surface of the waveguide was then etched using acetone to remove excess UPR and to reduce surface roughness. It is important to obtain low surface roughness to minimize light scattering which could cause high power loss [27]. At both ends of the waveguides, POF was attached which function to connect the waveguide to light source and light detector.

Characterization was done for RI response and temperature response in terms of sensitivity, and hysteresis. For RI response characterization, the sensors were immersed in glucose solution with various concentration which are 0%–12% which correspond to RI of 1.33 to 1.3547. LED with wavelength of 660 nm, serves as light source, was connected to the sensor through POF, while the output intensity was measured using VIS NIR spectrometer (Ocean Optics), as shown in Fig. 2(a). Temperature characterization were done by immersing the sensors in distilled water while heated using magnetic stirrer (DLAB H550S) with temperature variation of 35 °C–85 °C with increment of 5 °C as shown in Fig. 2(b).

3. Results and discussions

The fabricated waveguides were observed using charge coupled device (CCD) microscope, as shown in Fig. 3. It is shown that the core of sensor A and B have been fully filled with UPR. For sensor C, it is shown that the groove was half-filled by the core material. Output intensity measurement in air at room temperature show that the normalized output intensity of sensor A, B and C are −7.8 dB, −10.3 dB, and −12.9 dB, respectively, as shown in Fig. 4. Sensor C has the highest power loss due to dimension mismatch of POF and waveguide which results in high light scattering.

To obtain sensor sensitivity, characterization was done for two cycles. The average of normalized output intensity were plotted against RI values. As shown in Fig. 5, as the RI was increased, the output intensity decreased. The sensitivity of sensor A, B and C are −41.863 dB/RIU, −44.981 dB/RIU and −48.476 dB/RIU, respectively. By assuming that the spectral analyser has intensity resolution of 0.01 dB, the sensors resolution are 2.39 $\times 10^{-4}$ RIU, 2.22 $\times 10^{-4}$ RIU and 2.06 $\times 10^{-4}$ RIU for sensor A, sensor B and sensor C, respectively. The results are comparable with no-core optical fiber-based RI sensor which operated at visible light [28]. Clearly, sensor A provides the lowest sensitivity, while C has the highest sensitivity which is 16% higher than that of sensor A. For the half-filled core waveguide, the formed waveguide groove allow more light to interact with the environment. Therefore, the change of the environment's RI results in more effect to the output intensity of the half-filled core waveguide (sensor B) than the full-filled core waveguide (sensor A). The half-filled core sensor is similar to D-shaped fiber structure as proposed by Liu et al. [25] which has the highest sensitivity of −5.28 dB/RIU. Therefore, the proposed sensors provide 8.2 times higher sensitivity compared to

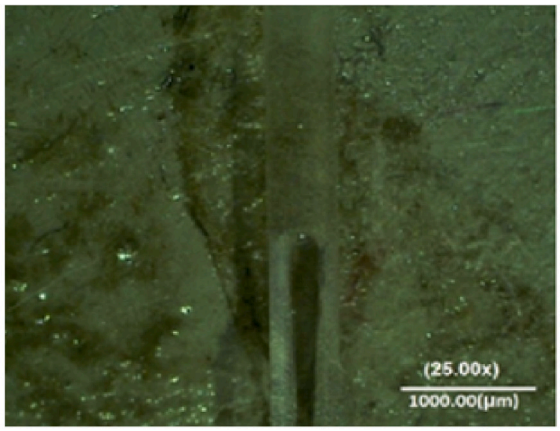

(a)

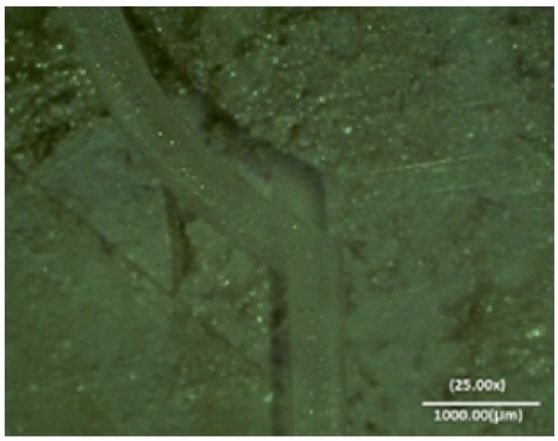

(b)

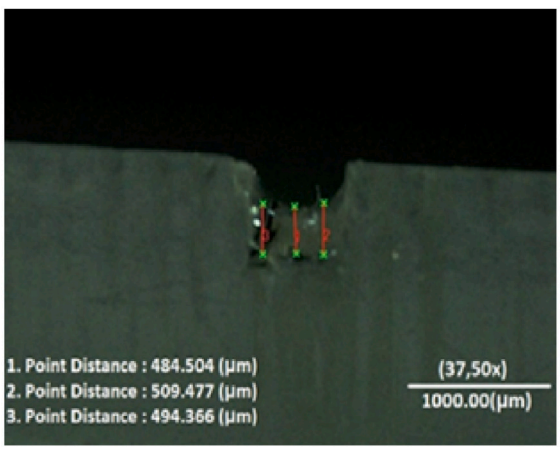

(c)

Fig. 3. CCD images of the fabricated waveguides: straight waveguide (a), curved waveguide (b) and half-filled core waveguide (d).

D-shaped fiber sensor. In terms of linearity, the sensors have good linearity with fitting coefficient (R2) of 0.983, 0.992 and 0.985 for sensor A, sensor B and sensor C, respectively.

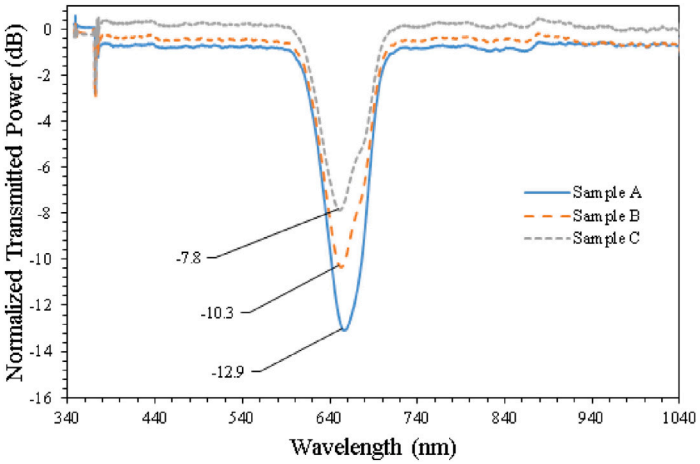

Fig. 4. Normalized transmitted power of the waveguides in air at room temperature.

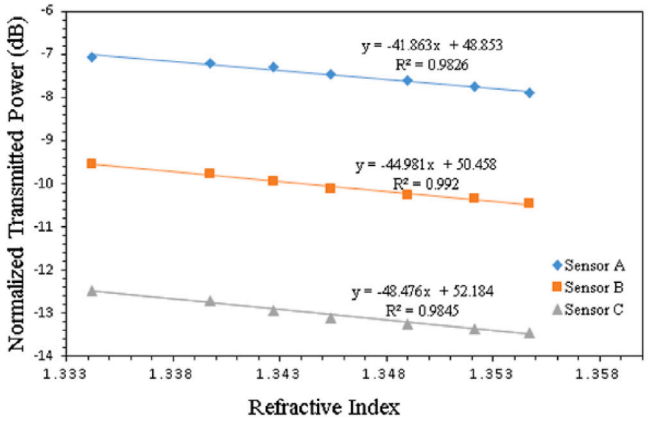

Fig. 5. Transmission vs. RI of sensor A, sensor B and sensor C. The gradients show the sensors' sensitivity.

Hysteresis (H) of the sensors were obtained by comparing the power loss from the increasing data and the decreasing data as defined by [29]

$$H = max((I(i) - D(i))/I(i)) \tag{1}$$

It was found that H for sensor A, sensor B and sensor C are 7.4×10^{-2}, 7.9×10^{-2} and 8.2×10^{-2}, respectively. Factors that might contribute to hysteresis are fluctuation of the light source intensity during measurement and noise of the detector. The hysteresis curves of each sensors are depicted in Fig. 6.

Temperature response of the sensors are depicted in Fig. 7. The output intensity increased as temperature increased due to the increase of numerical aperture (NA) [30]. Temperature sensitivity of sensor A, sensor B and sensor C are 8.9×10^{-3} dB/°C, 11.8×10^{-3} dB/°C and 15.8×10^{-3} dB/°C, respectively. It means that every environment temperature change will cause an error in RI measurement. Therefore, correction to compensate the temperature effect should be done.

Since the temperature response characterization was done in water, the above-measured temperature dependent loss was the effect of TOC and thermal expansion (TE) of the sensor and TOC of water. Hence, the RI measurement error due to the TOC and TE of the sensor only (ε_{RI}) is defined by

$$\varepsilon_{RI} = (S_T/S_{RI} - k_w)\,\text{RIU/°C} \tag{2}$$

where S_T, S_{RI} and k_w are the sensor temperature sensitivity, the sensor RI sensitivity and TOC of water, respectively. By taking TOC of water as -1.45×10^{-4} RIU/°C [31], the ε_{RI} for sensor A, sensor B and sensor C are -6.76×10^{-5} RIU/°C, -1.2×10^{-4} RIU/°C, and -1.8×10^{-4} RIU/°C, respectively. By measuring temperature of the observed liquid (T), correction could be done by deducing the measured RI (n_{meas}) with the calculated errors (ε_{RI}) to obtain the real RI (n_l) of the liquid, as defined by

$$n_l = n_{meas} - \varepsilon_{RI} T \tag{3}$$

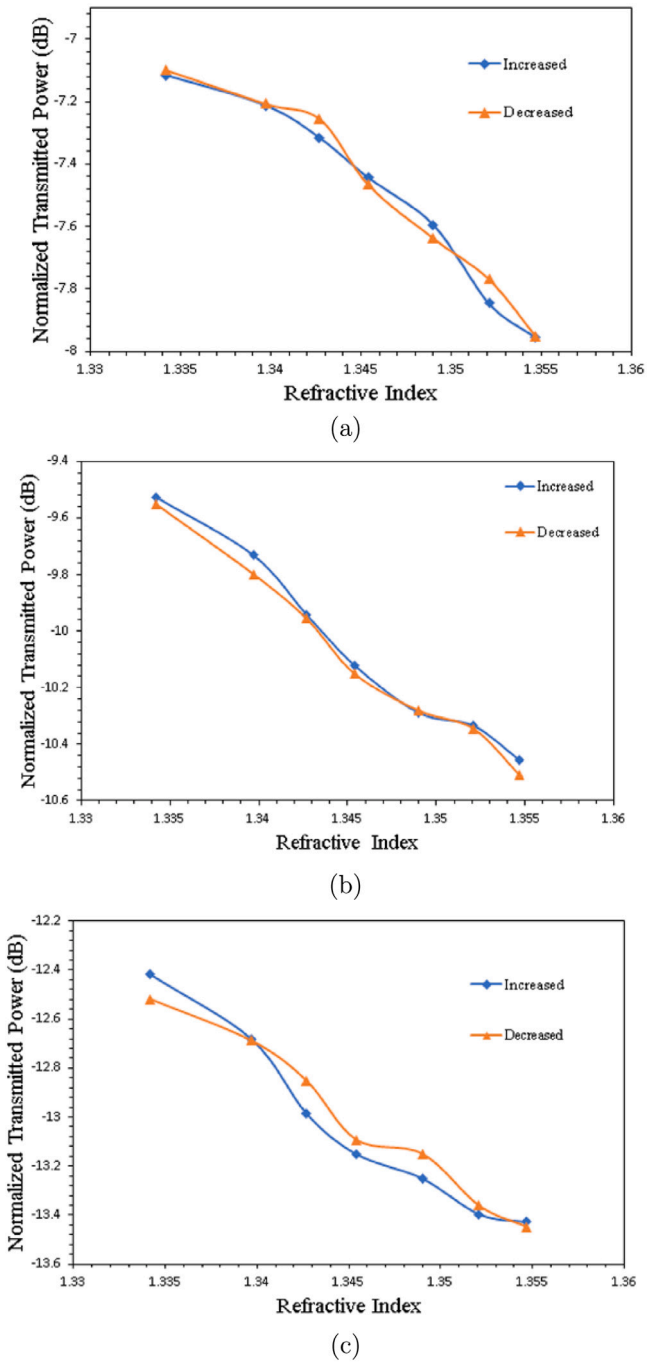

Fig. 6. Hysteresis curve of sensor A (a), sensor B (b) and sensor C (c).

For future work, it is important to design a single device for simultaneous measurement of RI and temperature to improve measurement efficiency.

4. Conclusions

UPR/PMMA based-SC waveguide for RI sensors have been fabricated using simple and low-cost fabrication technique. The sensors were design to be operated at wavelength of 660 nm. In addition to straight waveguide, curved waveguide and half-filled core waveguide were also fabricated to improve the sensor sensitivity. Characterization results showed that the sensors provide good

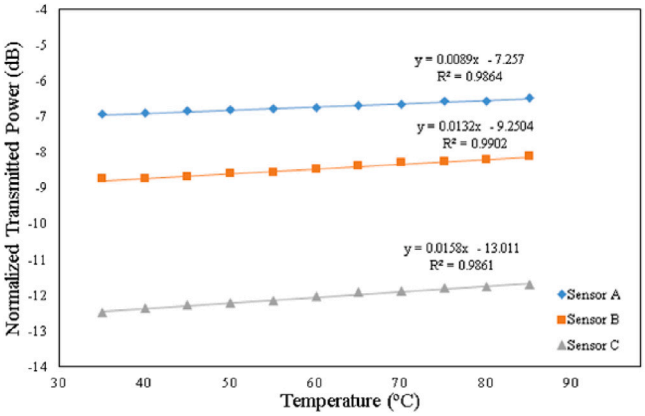

Fig. 7. Temperature response of sensor A, sensor B and sensor C.

performance in terms of sensitivity and linearity. Hysteresis was observed in the order of 10^{-2} which was occurred due to the light source fluctuation and detector noise. In terms of sensitivity, the half-filled core waveguide has the highest sensitivity which are −48.476 dB/RIU. However, it also has the highest hysteresis and the highest temperature dependency. The sensor accuracy could be further improved in future work by reducing the intensity fluctuation and by implementing temperature compensation.

Declaration of competing interest

The authors declare that they have no known competing financial interests or personal relationships that could have appeared to influence the work reported in this paper.

Acknowledgments

We would like to thank to Ministry of Education and Culture, Indonesia for funding the research through grant no 19.25.3/UN37/PPK.6.8/2021. Our gratitude also goes to the members of Physics Department, Universitas Negeri Semarang for their helpful discussion throughout the completion of this work.

References

[1] S. Maheswaran, P.G. Kuppusamy, S.M. Ramesh, T.V.P. Sundararajan, P. Yupapin, Refractive index sensor using dual core photonic crystal fiber – glucose detection applications, Results Phys. 11 (2018) 577–578, http://dx.doi.org/10.1016/J.RINP.2018.09.055.
[2] A. Gowri, A.S. Rajamani, B. Ramakrishna, V.V.R. Sai, U-bent plastic optical fiber probes as refractive index based fat sensor for milk quality monitoring, Opt. Fiber Technol. 47 (2019) 15–20, http://dx.doi.org/10.1016/J.YOFTE.2018.11.019.
[3] K. Ni, C.C. Chan, L. Chen, X. Dong, R. Huang, Q. Ma, A chitosan-coated humidity sensor based on Mach–Zehnder interferometer with waist-enlarged fusion bitapers, Opt. Fiber Technol. 33 (2017) 56–59, http://dx.doi.org/10.1016/j.yofte.2016.11.005.
[4] M. Danaie, B. Kiani, Design of a label-free photonic crystal refractive index sensor for biomedical applications, Photonics Nanostruct. - Fundam. Appl. 31 (2018) 89–98, http://dx.doi.org/10.1016/j.photonics.2018.06.004.
[5] W.-M. Zhao, Q. Wang, A high sensitivity refractive index sensor based on three-level gradient structure S-tapered fiber mode-mode interferometer, Measurement 139 (2019) 49–60, http://dx.doi.org/10.1016/J.MEASUREMENT.2019.03.018.
[6] J. Wang, B. Liu, Y. Wu, Y. Mao, L. Zhao, T. Sun, T. Nan, A novel fiber in-line michelson interferometer based on end face packaging for temperature and refractive index measurement, Optik (Stuttg.) 194 (2019) 163094, http://dx.doi.org/10.1016/J.IJLEO.2019.163094.
[7] Y. Li, Y. Miao, F. Wang, J. Wang, Z. Ma, L. Wang, X. Di, K. Zhang, Serial-tilted-tapered fiber with high sensitivity for low refractive index range, Opt. Express 26 (2018) 34776, http://dx.doi.org/10.1364/OE.26.034776.
[8] W. Li, A. Zhang, Q. Cheng, C. Sun, Y. Li, Theoretical analysis on SPR based optical fiber refractive index sensor with resonance wavelength covering communication C+L band, Optik (Stuttg.) 213 (2020) 164696, http://dx.doi.org/10.1016/j.ijleo.2020.164696.
[9] X. Lu, X. Zhang, N. Chen, M. Chang, B. Li, A high linearity refractive index sensor based on D-shaped photonic-crystal fiber with built-in metal wires, Optik (Stuttg.) 220 (2020) 165021, http://dx.doi.org/10.1016/j.ijleo.2020.165021.
[10] B. Pang, Z. Gu, Q. Ling, W. Wu, Y. Zhou, Simultaneous measurement of temperature and surrounding refractive index by superimposed coated long period fiber grating and fiber Bragg grating sensor based on mode barrier region, Optik (Stuttg.) 220 (2020) 165136, http://dx.doi.org/10.1016/j.ijleo.2020.165136.
[11] M. Gu, S. Yuan, Q. Yuan, Z. Tong, Temperature-independent refractive index sensor based on fiber Bragg grating and spherical-shape structure, Opt. Lasers Eng. 115 (2019) 86–89, http://dx.doi.org/10.1016/J.OPTLASENG.2018.11.018.
[12] W. Feng, Z. Gu, Ultrahigh-sensitivity fiber Bragg grating refractive index sensor based on thin cladding and mode transition, Optik (Stuttg.) 182 (2019) 341–348, http://dx.doi.org/10.1016/J.IJLEO.2019.01.025.
[13] W. Wang, H. Zhang, B. Li, Z. Li, Y. Miao, Optical fiber magnetic field sensor based on birefringence in liquid core optical waveguide, Opt. Fiber Technol. 50 (2019) 114–117, http://dx.doi.org/10.1016/j.yofte.2019.03.011.
[14] V.N. Konopsky, E.V. Alieva, Imaging biosensor based on planar optical waveguide, Opt. Laser Technol. 115 (2019) 171–175, http://dx.doi.org/10.1016/J.OPTLASTEC.2019.02.034.

[15] D. Niu, D. Zhang, L. Wang, T. Lian, M. Jiang, X. Sun, Z. Li, X. Wang, High-resolution and fast-response optical waveguide temperature sensor using asymmetric Mach–Zehnder interferometer structure, Sensors Actuators A 299 (2019) 111615, http://dx.doi.org/10.1016/j.sna.2019.111615.
[16] X. Ma, K. Chen, J. Wu, L. Wang, Low-cost and highly sensitive liquid refractive index sensor based on polymer horizontal slot waveguide, Photonic Sensors 10 (2020) 7–15, http://dx.doi.org/10.1007/s13320-019-0560-y.
[17] B. Wang, Q. Wang, L. Kong, R. Lv, Graphene oxide-polymethylmethacrylate polymer waveguide device based on near infrared fingerprint spectrum for refractive index sensing, Trans. Inst. Meas. Control 40 (2017) 2607–2610, http://dx.doi.org/10.1177/0142331217707364.
[18] W. Du, F. Zhao, Surface plasmon resonance based silicon carbide optical waveguide sensor, Mater. Lett. 115 (2014) 92–95, http://dx.doi.org/10.1016/J.MATLET.2013.10.035.
[19] L. Ji, S. Yang, R. Shi, Y. Fu, J. Su, C. Wu, Polymer waveguide coupled surface plasmon refractive index sensor: A theoretical study, Photonic Sensors 10 (2020) 353–363, http://dx.doi.org/10.1007/s13320-020-0589-y.
[20] L. Ji, W. Wei, G. Li, S. Yang, Y. Fu, J. Su, C. Wu, Refractive index sensor based on metal-clad planar polymer waveguide operating at 850 nm, Photonic Sensors (2020) http://dx.doi.org/10.1007/s13320-020-0606-1.
[21] R.M. Pope, E.S. Fry, Absorption spectrum (380–700 nm) of pure water. II. Integrating cavity measurements, Appl. Opt. 36 (1997) 8710–8723, http://dx.doi.org/10.1364/AO.36.008710.
[22] B. Hooda, V. Rastogi, Low cost highly sensitive miniaturized refractive index sensor based on planar waveguide, Optik (Stuttg.) 143 (2017) 158–166, http://dx.doi.org/10.1016/J.IJLEO.2017.06.050.
[23] I. Yulianti, J. Azka, N.M. Darma Putra, B. Astuti, Buried waveguide polymethylmethacrylate modeling for refractive index sensor application using finite element method, Spektra J. Fis. Dan Apl. 4 (2019) 133–142, http://dx.doi.org/10.21009/spektra.043.04.
[24] D.M.C. Rodrigues, R.C.S.B. Allil, V.M. Queiroz, R.N. Lopes, M.M. Werneck, Investigation of different shapes of plastic optical fiber sensor for refractometry and detection of bacteria, in: 2015 IEEE Int. Instrum. Meas. Technol. Conf. Proc., 2015, pp. 171–175, http://dx.doi.org/10.1109/I2MTC.2015.7151260.
[25] G. Liu, D. Feng, Evanescent wave analysis and experimental realization of refractive index sensor based on D-shaped plastic optical fiber, Optik (Stuttg.) 127 (2016) 690–693, http://dx.doi.org/10.1016/j.ijleo.2015.10.129.
[26] I.-C. Liu, P.-C. Chen, L.-K. Chau, G.-E. Chang, Optofluidic refractive-index sensors employing bent waveguide structures for low-cost, rapid chemical and biomedical sensing, Opt. Express 26 (2018) 273–283, http://dx.doi.org/10.1364/OE.26.000273.
[27] F. Sequeira, N. Cennamo, A. Rudnitskaya, R. Nogueira, L. Zeni, L. Bilro, D-shaped POF sensors for refractive index sensing—The importance of surface roughness, Sensors 19 (2019) http://dx.doi.org/10.3390/s19112476.
[28] Z. Ding, C. Zhao, T. Lang, J. Jin, Fiber refractive index sensor based on surface plasmon resonance with no-core fiber, in: 2017 Conf. Lasers Electro-Optics Pacific Rim, 2017, pp. 1–3, http://dx.doi.org/10.1109/CLEOPR.2017.8118671.
[29] M.S. Avila-Garcia, M. Bianchetti, R. Le Corre, A. Guevel, R.I. Mata-Chavez, J.M. Sierra-Hernandez, D. Jauregui-Vazquez, J.R. Reyes-Ayona, J.M. Estudillo-Ayala, R. Rojas-Laguna, High sensitivity strain sensors based on single-mode-fiber core-offset Mach–Zehnder interferometers, Opt. Lasers Eng. 107 (2018) 202–206, http://dx.doi.org/10.1016/J.OPTLASENG.2018.02.008.
[30] A. Tapetado, P.J. Pinzón, J. Zubia, C. Vázquez, Polymer optical fiber temperature sensor with dual-wavelength compensation of power fluctuations, J. Lightwave Technol. 33 (2015) 2716–2723, http://dx.doi.org/10.1109/JLT.2015.2408368.
[31] C. Teng, F. Yu, N. Jing, J. Zheng, The influence of temperature to a refractive index sensor based on a macro-bending tapered plastic optical fiber, Opt. Fiber Technol. 31 (2016) 32–35, http://dx.doi.org/10.1016/j.yofte.2016.05.009.